Probing the properties of metal–oxide interfaces: silica films on Mo and Ru supports

2012 J. Phys.: Condens. Matter 24 354010

(http://iopscience.iop.org/0953-8984/24/35/354010)

IOP Publishing Journal of Physics: Condensed Matter
J. Phys.: Condens. Matter **24** (2012) 354010 (7pp) doi:10.1088/0953-8984/24/35/354010

Probing the properties of metal–oxide interfaces: silica films on Mo and Ru supports

Leonid Lichtenstein, Markus Heyde, Stefan Ulrich, Niklas Nilius and Hans-Joachim Freund

Fritz-Haber-Institute of the Max-Planck-Society, Faradayweg 4–6, D-14195 Berlin, Germany

E-mail: nilius@fhi-berlin.mpg.de

Received 9 March 2012
Published 16 August 2012
Online at stacks.iop.org/JPhysCM/24/354010

Abstract
The influence of metal–oxide interactions on the workfunction and band alignment in thin oxide films is investigated for silica mono- and bilayers grown on Mo(112) and Ru(0001) supports. By analyzing the position of field-emission resonances and the Kelvin-probe signal deduced from conductance and force spectroscopy, we have identified a substantial lowering of the workfunction in the monolayer films, with the oxide bands shifting accordingly. We explain this observation with a stronger coupling and a shorter binding length of the silica monolayer to the metal substrate, which removes the effect of electron spill-out, produces a positive interface dipole and reduces the workfunction of the system. In contrast, the van der Waals bound bilayer film interacts only weakly with the Ru support, conserving the effect of electron spill-out and keeping the workfunction high. Direct evidence for the relevance of interface interactions comes from experiments on buckled silica films, for which regular workfunction modulations are revealed that follow the topographic height of the film above the metal surface.

(Some figures may appear in colour only in the online journal)

1. Introduction

Thin oxide films on metal supports have been widely used as model systems for the respective bulk oxides that would be difficult to investigate via conventional surface-science techniques otherwise due to their insulating nature [1–3]. However, thin oxide films are fascinating systems in their own right, as they exhibit unique properties that can neither be found on metals nor on oxide surfaces, but reflect the genuine mixture of both characteristics [4, 5]. Moreover, the preparation of crystalline oxide layers on metal substrates is a powerful approach to study the nature of interface interactions between both kinds of materials [6, 7]. Finally, once the nature of interface coupling has been elucidated, new possibilities for tailoring the physical and chemical properties of metal–oxide systems may be accessible, resulting in novel materials with unexpected functionalities [8]. Already today, a large number of applications are based on specific effects occurring at metal–oxide interfaces, such as low workfunction electron emitters [9], dielectric layers for optical devices and thin films for corrosion protection [10]. The most relevant applications lie, however, in the field of supported metal catalysts, where not the metal particles themselves but thin oxide films that spontaneously grow at reaction conditions are considered to be the catalytically active phase [11, 12].

There are many possible coupling regimes occurring at metal–oxide interfaces. The strongest one is direct hybridization between metal and oxide states across the interface, as revealed, for example, for thin alumina films on NiAl(110), where the interface oxide plane is already part of the original metal surface [13]. In most cases, however, interface interactions are weak as direct hybridization across the interface is inhibited by the large bandgap and the chemically saturated nature of the oxide ions. In those cases, electrostatic interactions mediate the interface coupling, such as polarization and charge transfer

effects [14–17]. A dominance of Coulomb-type interactions has been identified for many rocksalt-type oxides on noble metal supports, e.g. for MgO on Ag(111) and Pd(100) and for FeO on Pt(111) [18]. The most relevant fingerprint of electrostatic interactions is a change in the workfunction of the metal–oxide systems due to the development of interface dipoles [16, 19, 20]. In fact, those workfunction changes are also in the center of many applications discussed before, as they enable an electron exchange across the metal–oxide interface that may constitute the initial step for a catalytic reaction [21].

In this study, we have investigated the interface properties between different silica films and either Mo(112) or Ru(0001) supports. Using scanning tunneling microscopy (STM) and atomic force microscopy (AFM), we have analyzed the potential situation at the interface and the presence of interface dipoles. Surprisingly, we found that chemically similar silica mono- and bilayer structures may exhibit pronounced differences in the nature of their interface, giving rise to different workfunctions and band alignments. We ascribe these effects to the interplay of various interface dipoles that develop as a consequence of the metal–oxide interactions.

2. Experimental details

The experiments were carried out in two ultrahigh-vacuum scanning probe systems operated at liquid helium temperature. While the first one is a tunneling microscope, the second combines tunneling and atomic force capabilities as the sensor is made of a quartz tuning fork with a metal tip attached to one prong [22]. By this means, electronic and force signals can be detected simultaneously, providing topographic and electrostatic information within one experiment. Insight into the electronic structure of the sample was obtained with conductance spectroscopy performed with a lock-in technique [23]. The workfunction was measured by a variation of the Kelvin probe technique, performed with the oscillating metal tip at the tuning fork sensor [24].

The three silica films discussed in this paper have been grown on two different substrates, using slightly different preparation procedures. The first one, referred to as Mo-ML for a Mo-supported monolayer, has been grown by dosing 1.4 ML Si onto an oxygen pre-covered Mo(112) surface in 2×10^{-7} mbar O_2 at room temperature [25]. Crystallization of the film was achieved by vacuum annealing to 1200 K, producing a sharp (2 × 2) pattern in low-energy electron diffraction (LEED). The other two films were grown on a Ru(0001) support, cleaned via Ar^+ sputtering and annealing to 1600 K. Silicon was deposited in 2×10^{-7} mbar O_2 at 570 K, followed by an annealing step to 1170 K in 2×10^{-6} mbar oxygen. Depending on the initial Si load and the cooling speed after the final heating, either a crystalline monolayer [26] or an amorphous bilayer film [27] was produced. Whereas a sharp (2×2) LEED pattern was observed in the first case, only a ring feature appeared in the latter, indicating rotational disorder of the Si–O units in the silica bilayer.

3. Results and discussion

STM topographic images of the different silica films are displayed in figures 1(a)–(c). Evidently, all three films have a porous structure, i.e. they contain nanometer-sized holes reaching down to the metal support. Whereas in the Mo-ML and Ru-ML, the pores form a long-range-ordered hexagonal pattern of 5.5 Å periodicity, pores of different sizes and without spatial regularity appear in the Ru-BL. However, the fundamental building blocks, being SiO_4 tetrahedra, are identical in all three cases. According to density functional (DFT) calculations, six SiO_4 units combine into a hexagonal ring in the two monolayer films [25], while four- to nine-membered rings are found in the amorphous Ru-BL [27]. The driving force for the formation of either crystalline or amorphous silica is the different amounts of interface coupling in the mono- and bilayer case (figures 1(d)–(f)). In the silica monolayers, one O ion of each SiO_4 tetrahedron binds to the metal surface and enforces the development of an interfacial registry. In the Ru-BL, on the other hand, two sheets of SiO_4 tetrahedra are interconnected via O ions and no chemical bond is formed to the metal beneath. Already small deviations from thermodynamic equilibrium are thus sufficient to perturb the crystallization process, explaining the large tendency of the Ru-BL to develop an amorphous structure. As a consequence of the different interface interactions, the mean distance between the metal surface and the oxide film differs substantially in the mono- and bilayer case. Whereas the first O plane lies only 1.4 Å above the last layer of Mo atoms in the Mo-ML (corresponding to a Mo–O bond length of 2.0 Å) [25], this value increases to 1.8 Å in the Ru-ML system and to 3.8 Å for the Ru-BL [35]. The enlargement of the interface distance when going from mono- to bilayer films also marks the transition between chemically and van der Waals coupled systems.

3.1. Field-emission resonance spectroscopy

The different binding geometries of the three films give rise to changes in their electronic structure and in the potential course across the metal–oxide interface that can be accessed by means of conductance [28] and Kelvin probe spectroscopy [29]. In the STM mode, the workfunction is deduced indirectly from the energy position of field-emission resonances (FERs) that develop in the tip–sample contact at high bias (figure 2(a)) [30]. In simple terms, the FERs can be considered as eigenstates in a triangular quasi-potential delimited by the sample surface and the down-sloping vacuum barrier (figure 2(b)). Electrons that enter this classically allowed region produce standing waves, if multiples of their half-wavelength match the distance between the two boundaries. In this case, incident and reflected waves interfere constructively, resulting in quasi-bound electronic states with high transmissibility for electrons. The bottom of the quasi-potential is given by the sample workfunction and the position of the FERs may thus be used to probe this quantity at a local scale [28, 29]. A downshift of the FER energies thereby indicates a decline of the workfunction and already the

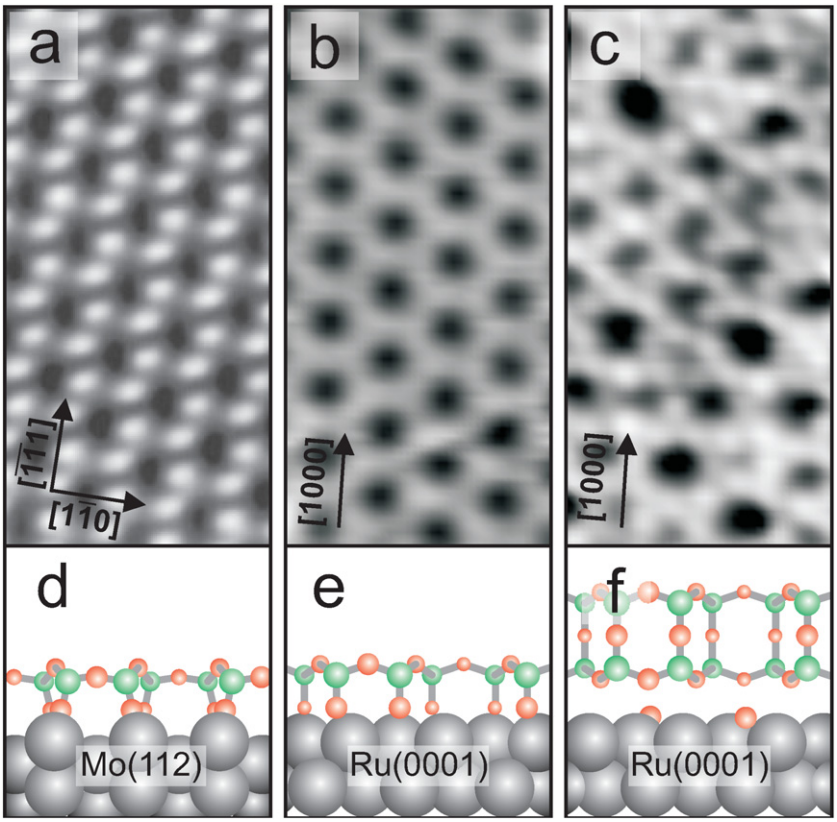

Figure 1. STM topographic images (20×40 Å^2) and corresponding structure models of the three silica films discussed in this paper: ((a), (d)) Mo-ML, ((b), (e)) Ru-ML and ((c), (f)) Ru-BL.

position of the first resonance gives an insight into qualitative trends. A quantitative approximation might be obtained from fitting the higher resonance energies E_n as a function of their peak order n according to: $E_n = \Phi + cn^{2/3}$, with Φ being the workfunction and c a proportionality factor [31]. We note that the first resonance is typically discarded from the fitting, as its position is not only governed by the nature of the triangular potential but also by image-potential interactions between the electrons and the surface.

A series of FER spectra taken on the three silica films as well as on the bare and oxygen-covered Ru(0001) is shown in figure 2. All spectra have been acquired in the constant-current mode with enabled feedback loop, and each maximum marks a FER in the tip–sample gap. Evidently, the bias position of the first and higher resonances varies substantially for the different samples (figure 2(c)). On the bare metal, the FERs start at around 5.5 V but shift to 6.4 V upon oxygen exposure [32]. A similar behavior is found for bare Mo(112), only that the onset of the FERs is systematically downshifted by 1.0 V (not shown). With a monolayer film on top, the onset of the FERs moves to 4.3 and 4.65 V for the Mo and Ru support, respectively. For the Ru-BL, finally, the FERs shift up again and are now detected above 5.5 V as for the clean Ru. Apparently, the monolayer silica films have the lowest FERs, and hence the lowest workfunction, while the bilayer and O-covered surfaces feature high Φ values. The picture changes slightly when the higher resonances are included in the workfunction analysis. The monolayer films on Mo(112) and Ru(0001) now have Φ values that are 1.0 and 1.8 eV lower than the Ru reference, respectively, while the bilayer has a similar workfunction. However, the fitting procedure is not very accurate due to the small number of FERs in the accessible bias window of 1–10 V. In particular, absolute Φ values are often too low, while relative changes are reproduced rather well [28].

3.2. Kelvin-probe spectroscopy

This technique was applied for workfunction measurements on the Ru-supported silica films, because only this sample system has been investigated with the combined STM–AFM set-up. The following procedure was used to extract relative Φ values from the experimental data. The tip and sample were contacted via the electronics to align their Fermi levels, which causes an electric field to occur between the tip and sample. The associated electrostatic force shifts the resonance frequency of our tuning-force sensor to lower values, as determined by fitting the frequency versus bias curves with a parabolic function. The bias difference of the frequency maxima in spectra taken for the Ru-ML and Ru-BL now corresponds to the shift in the electrostatic potential between the two situations (figure 3). As contact potential measurements depend on the local tip geometries, we have acquired all data with one and the same microscopic tip configuration. The so-determined contact potentials amount to 1.40 and 1.47 eV for the Ru-ML and Ru-BL, respectively

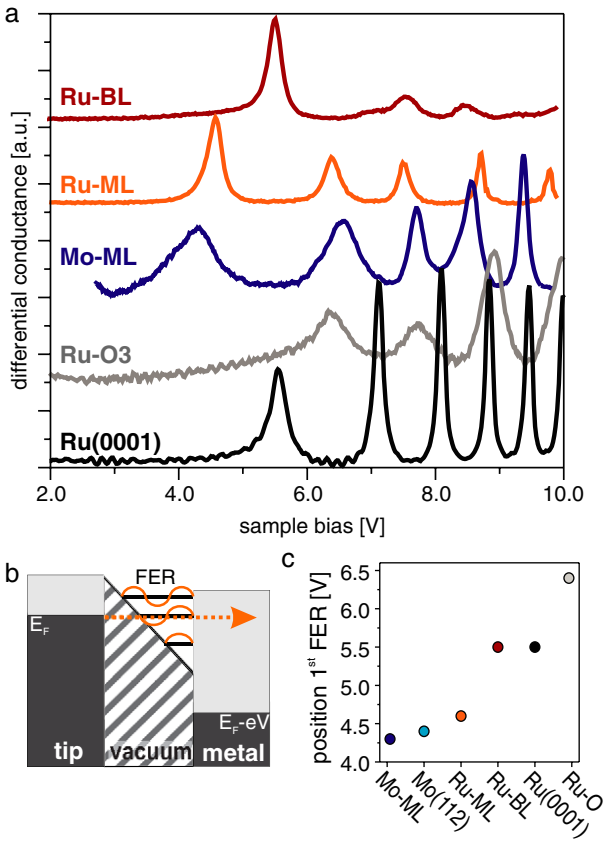

Figure 2. (a) STM conductance spectra taken in the region of the field-emission resonances (FERs) for different silica thin films as well as for Ru and Ru–O. (b) Potential diagram of the STM junction explaining the formation of the FERs at high bias. (c) Position of the first FER that gives a rough measure of the sample workfunction on the different surfaces.

(figure 3, inset). Consequently, Kelvin-probe spectroscopy confirms the higher workfunction of the silica bilayer, although the shift is much smaller than in the FER data. We explain this relatively small shift with the limited spatial resolution of the Kelvin-probe method that leads to an interference of ML and BL signals as both regions coexist on the surface.

3.3. Band edge spectroscopy

In a last approach, we have determined the band positions in mono- and bilayer films in order to analyze the potential situation at the metal–oxide interface. As bands in weakly-coupled oxide films adjust themselves to the vacuum energy, changes in this quantity cause the band positions to shift against the metal Fermi level. The onsets for the valence (VB) and conduction band (CB) have been probed with STM conductance spectroscopy, where they produce small shoulders in the exponential increase of the conductance signal. After subtracting this background, the onset position can be determined with good accuracy (figure 4). For the Mo-ML, the VB and CB onsets have been determined with -3.9 and $+2.8$ V, respectively, yielding a total bandgap of 6.7 V. For the Ru-BL, the bands shift to VB $= -2.7$ V and CB $= +3.8$ V and the total gap becomes slightly smaller. The

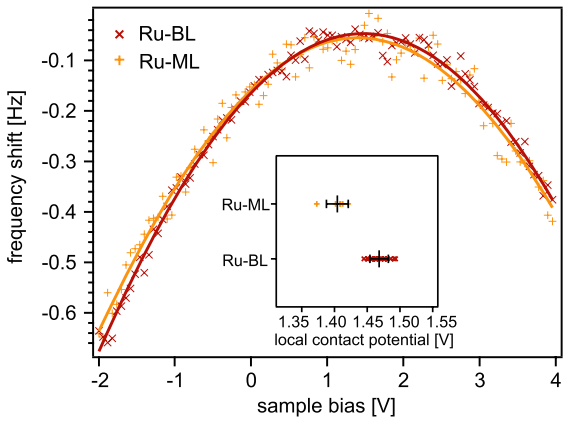

Figure 3. Frequency shift versus bias spectroscopy on Ru-ML (bright) and Ru-BL (dark) films. The curves were fitted with a parabola to determine the contact potentials. The resulting values are depicted in the inset, while the error bars represent the standard deviation determined from multiple experiments.

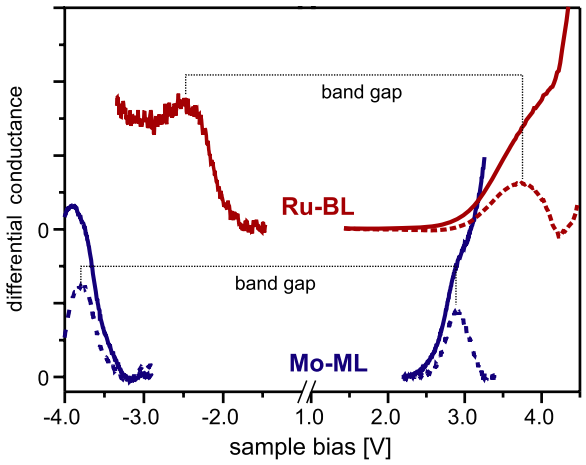

Figure 4. STM conductance spectra taken in the region of the valence and conduction band onsets of Mo-ML and Ru-BL films. The solid lines mark the original data, while the dashed lines have been obtained after subtracting an exponential background that accounts for the exponentially decreasing tunnel barrier at high bias.

two bandgaps are therefore smaller than the silica bulk gap of 8.7 eV, reflecting the reduced dimensionality of the thin films. We further note a considerable up-shift of the band edges when going from mono- to bilayer films, indicating again a higher vacuum energy and a higher workfunction for the Ru-BL. No band positions could be detected for the Ru-ML, as oxide-related changes in the conductance signal were too small to be distinguished from tunneling processes into the Ru metal.

In summary, the different STM and AFM-based methods provided consistent spectroscopic evidence for a lower workfunction in monolayer than in bilayer silica films grown on Mo and Ru substrates. We will rationalize this behavior in the following paragraphs.

3.4. Discussion

The potential course at metal–oxide interfaces arises from the interplay of three coupled electrostatic dipoles [16, 19].

The first one, p_{film}, reflects the charge distribution inside the isolated oxide film, i.e. without metal support. In the monolayer silica films, it points with its positive end to the vacuum, as positive and negative charge centers are located in the surface and interface plane, respectively. The bilayer film, on the other hand, is perfectly dipole-compensated and p_{film} equals zero. The second dipole, p_{inter}, comes into play when placing the film onto a metal support and allowing electrons to flow across the interface. The direction and amount of this charge exchange is governed by the electron affinities of the silica films in our case, as Mo and Ru have comparable affinity values. The monolayer films share four O ions per (2×2) unit cell with the support, which attract electrons from the metal into their O 2p orbitals. The bilayer film, on the other hand, is chemically saturated and no substantial electron transfer is expected. Finally, the third dipole, p_{comp}, describes the alteration of the surface dipole that is inherently present on each metal due to spill-out of its electrons into a near-vacuum region. The oxide film compresses this dipole by exerting Pauli repulsion onto the surface electrons, an effect that always lowers the workfunction. We note that all three dipoles mutually influence each other. For example, a strong interface p_{inter} increases the rumpling of the film p_{film} in order to balance the two contributions [19].

Based on these considerations, the workfunction effects induced by the different silica films may be explained. On bare metals, the workfunction is governed by the electron spill-out that is more pronounced on close-packed than on highly corrugated and open surfaces, as is evident from the different Φ values of Ru(0001) (5.5 eV) and Mo(112) (4.5 eV) [33]. Producing an oxygen ad-layer causes the workfunction to rise, as the electronegative nature of oxygen reinforces the effect of electron spill-out at the metal surface. Conversely, the compression effect becomes dominant once a silica monolayer is grown on the metal surface and the workfunction declines again. The trend is largest for the Ru-ML where Φ drops by more than 1.0 eV with respect to bare Ru. On the Mo-ML, Φ reduces only by 0.2 eV, as the impact of p_{comp} is balanced by a larger interface dipole, resulting from a substantial electron flow into the interface O ions of the film. The deviation from the Ru-supported film is explained by the high oxygen affinity and the larger heat of oxidation of Mo compared to Ru [34]. Finally, the workfunction turns back to the free-metal value when transforming a mono- into a bilayer film, because of two reasons. First, the nature of the interface interaction changes from chemical to van der Waals-like, which suppresses any charge transfer and cancels the impact of p_{inter}. Second, the interface distance increases substantially in the bilayer case, providing sufficient space for the electron spill-out to take place again ($p_{\text{comp}} \rightarrow 0$). The similar Φ values for bare and silica-covered Ru are therefore not unexpected but reflect the chemically decoupled and electrostatically compensated nature of the bilayer film. We note that one factor has been excluded from our discussion so far, which is the possibility to stabilize extra oxygen at the metal–silica interfaces. As shown in a recent electron spectroscopy work [35], oxygen-poor and oxygen-rich interfaces can be produced for both the Mo-ML and Ru-BL systems. The extra O atoms attract more electrons from the metal surface, increasing p_{inter} and therewith the workfunction. The upper limit for this Φ shift is reached at the 3O (2×2) saturation coverage of oxygen at the interface, when a further Φ increase by around 1.0 eV is revealed with respect to the O-poor situation [35]. As we were unable to probe the extra oxygen in our study, we have not investigated this effect in detail.

3.5. Workfunction modulations across oxide films

The mutual interplay of the interface dipoles becomes not only evident for different oxide films, but can be probed for one, yet structurally inhomogeneous, layer, as discussed in this section. Such samples can be produced by annealing a Mo-ML to temperatures just below sublimation (1300 K) when certain oxide regions start to be lifted from the metal support. Respective STM images show a buckled morphology, in which high- and low-lying silica patches alternate in a regular fashion (figure 5). The crests of the resulting wavy pattern always align with a $\langle \bar{3}11 \rangle$ direction of Mo(112), i.e. with a diagonal of the silica unit-cells. Which of the two possible directions is adopted is decided by the orientation of nearby step edges. The lateral distance between two neighboring crests amounts to 40 Å, while the height modulation is as small as 0.3 Å (figure 5(b)). We assign the crests of the wavy pattern to oxide regions that have partly detached from the metal surface and therefore exhibit a reduced interface interaction. The driving force for the buckling is the misfit strain induced by a 8% smaller Mo(112) lattice constant with respect to the one of bulk silica. The periodicity and orientation of the pattern may be explained by assuming that ten silica rings overgrow two extra Mo(112) unit cells along a $\langle \bar{3}11 \rangle$ direction as compared to the epitaxial situation. This provides roughly 9% more space for each silica ring and effectively removes the misfit strain. However, the buckling brings about that only the low-lying film regions can realize their preferred interface registry, while the upper ones have an incommensurate relationship with the Mo surface.

Although the vertical displacements in buckled Mo-ML films are tiny (0.3 Å), the impact on the electronic structure is immense, as shown with conductance images measured as a function of the bias voltage (figures 5(c)–(h)). At low bias, the maps are featureless because the electrons tunnel through the silica bandgap. However, a pronounced contrast that follows the wavy pattern in the topography appears once the onset of the oxide conduction band is reached at 2.8 V. Whereas the low-lying patches turn bright at this condition, the upper ones retain their original small $\mathrm{d}I/\mathrm{d}V$ intensity. Apparently, the tip electrons reach the oxide CB and therewith a high state density for tunneling in the low-lying parts of the film, but still have to pass the full bandgap in the elevated regions. This observation perfectly matches the concept developed before. At small interface distances, the electron spill-out from the Mo metal is suppressed and p_{comp} is positive, leading to a workfunction decline and a downshift of the oxide bands. Consequently, the CB edge is already reached at 2.8 V and the low-lying oxide regions appear bright in the $\mathrm{d}I/\mathrm{d}V$ maps. In

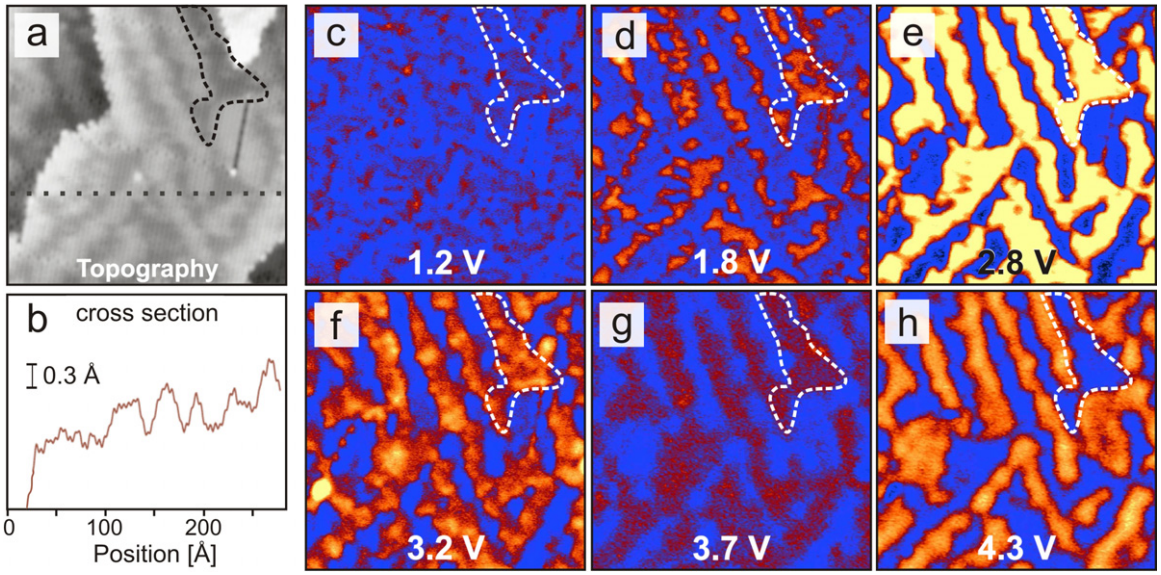

Figure 5. Morphology (a) and conductance maps ((c)–(h)) of a Mo-ML film that has been annealed to 1300 K to stimulate buckling (300×300 Å^2). Dark (blue) and red (bright) colors denote low and high dI/dV signals in the conductance maps. A particularly strong contrast is revealed at the conduction band onset (2.8 V) and at the position of the first FER (4.3 V). (b) Height profile taken along the dotted line in (a).

contrast, electron spill-out becomes possible on the elevated regions of the film and workfunction and band positions shift upward. The latter effect explains the reduced dI/dV contrast of the high-lying areas in maps taken close to the CB onset at 2.8 V. At higher bias, the contrast between low- and high-lying silica patches reverses, which is, however, a pure geometric and not an electronic effect. The dI/dV contrast above 4.0 V is governed by the FERs, which are reached first above the elevated parts of the Mo-ML, where the tip–metal distance is larger and the triangular potential that accommodates the FERs is wider. A wider potential now causes the FER levels to shift down in energy, explaining why the FER-mediated contrast enhancement affects the elevated oxide regions first.

The contrast modulations revealed in the dI/dV maps of buckled Mo-ML films have therefore the same origin as the workfunction shift between mono- and bilayer films. With increasing interface distance, the effect of electron spill-out becomes dominant which leads to an up-shift of both the workfunction and the band onsets. The fact that already height modulations as small as 0.3 Å produce measurable effects in the conductance maps highlights the sensitivity of the electronic properties on the precise interface geometry [19].

4. Conclusions

The potential course and resulting workfunction effects have been explored for different silica–metal interfaces, using STM- and AFM-based spectroscopic techniques. Despite uncertainties in the quantitative values, we reproducibly observed a lower workfunction for silica mono- compared to bilayer films. We assign this difference to variations in the electron spill-out at the respective metal–oxide interface, following earlier concepts developed by DFT [16, 19]. In the case of strong interface coupling, the Pauli repulsion exerted by the oxide overlayer reduces the effect of electron spill-out and the workfunction is low. For van der Waals coupled systems, on the other hand, the spill-out is fully developed and the workfunction rises again. Alternations between low and high workfunction regions have been detected for buckled Mo-ML films that exhibit periodic variations of the interface distance.

The elucidation of interface phenomena that govern the workfunction of thin-film systems is a first step to control this important parameter, e.g. by changing the metal substrate used for oxide growth. Given the importance of the workfunction in charge transfer processes, this possibility opens fascinating routes to tailor the performance of thin-film systems in chemical reactions. Moreover, spatial variations in Φ might be exploited to trigger self-organization effects of suitable adsorbates on the oxide surface, being a step towards surface patterning and device fabrication [36]. Based on the experimental results presented here, we note that substantial workfunction variations might occur even on chemically homogeneous samples, emphasizing the need to probe this quantity at a local scale. Some approaches for local workfunction mapping have been introduced in this paper; however, all of them are unable to provide reliable absolute Φ values. Further efforts are therefore requested to overcome this unsatisfying situation.

Acknowledgment

The authors acknowledge support from the DFG within the Cluster of Excellence ‘UniCat’.

References

[1] Street S C, Xu C and Goodman D W 1997 *Annu. Rev. Phys. Chem.* **48** 43–68
[2] Baumer M and Freund H-J 1999 *Prog. Surf. Sci.* **61** 127–98

[3] Chambers S A 2000 *Surf. Sci. Rep.* **39** 105–80
[4] Risse T, Shaikhutdinov S, Nilius N, Sterrer M and Freund H-J 2008 *Acc. Chem. Res.* **41** 949–56
[5] Freund H-J and Pacchioni G 2008 *Chem. Soc. Rev.* **37** 2224–42
[6] Fu Q and Wagner T 2007 *Surf. Sci. Rep.* **62** 431–98
[7] Ernst F 1995 *Mater. Sci. Eng.* R **14** 97–156
[8] Martinez U, Jerratsch J F, Nilius N, Giordano L, Pacchioni G and Freund H-J 2009 *Phys. Rev. Lett.* **103** 056801
[9] Nemeth K, Harkay K C, van Veenendaal M, Spentzouris L, White M, Attenkofer K and Srajer G 2010 *Phys. Rev. Lett.* **104** 046801
[10] Jones D A 1995 *Principles and Prevention of Corrosion* (Upper Saddle River, NJ: Prentice-Hall)
[11] Hendriksen B L M and Frenken J W M 2002 *Phys. Rev. Lett.* **89** 046101
[12] Lewandowski M, Sun Y N, Qin Z H, Shaikhutdinov S and Freund H J 2010 *Appl. Catal.* A **391** 407–10
[13] Kresse G, Schmid M, Napetschnig E, Shishkin M, Köhler L and Varga P 2005 *Science* **308** 1440
[14] Goniakowski J and Noguera C 2004 *Interface Sci.* **12** 93
[15] Giordano L, Goniakowski J and Pacchioni G 2003 *Phys. Rev.* B **67** 045410
[16] Giordano L, Cinquini F and Pacchioni G 2006 *Phys. Rev.* B **73** 045414
[17] Honkala K and Hakkinen H 2007 *J. Phys. Chem.* C **111** 4319–27
[18] Giordano L, Pacchioni G, Goniakowski J, Nilius N, Rienks E D L and Freund H-J 2007 *Phys. Rev.* B **76** 075416
[19] Goniakowski J and Noguera C 2009 *Phys. Rev.* B **79** 155433
[20] Pivetta M, Patthey F, Stengel M, Baldereschi A and Schneider W D 2005 *Phys. Rev.* B **72** 115404
[21] Hellman A, Klacar S and Gronbeck H 2009 *J. Am. Chem. Soc.* **131** 16636
[22] Heyde M, Simon G H, Rust H-P and Freund H-J 2006 *Appl. Phys. Lett.* **89** 263107
[23] Tersoff J and Hamann D 1985 *Phys. Rev.* B **31** 805
[24] Nonnenmacher M, O'Boyle M P and Wickramasinghe H K 1991 *Appl. Phys. Lett.* **58** 2921–3
[25] Weissenrieder J, Kaya S, Lu J L, Gao H J, Shaikhutdinov S, Freund H-J, Sierka M, Todorova T K and Sauer J 2005 *Phys. Rev. Lett.* **95** 076103
[26] Löffler D *et al* 2010 *Phys. Rev. Lett.* **105** 146104
[27] Lichtenstein L, Büchner C, Yang B, Shaikhutdinov S, Heyde M, Sierka M, Włodarczyk R, Sauer J and Freund H-J 2012 *Angew. Chem. Int. Edn* **51** 404–7
[28] Rienks E D L, Nilius N, Rust H-P and Freund H-J 2005 *Phys. Rev.* B **71** 241404
[29] König T, Simon G H, Rust H-P and Heyde M 2009 *J. Phys. Chem.* C **113** 11301–5
[30] Binnig G, Frank K H, Fuchs H, Garcia N, Reihl B, Rohrer H, Salvan F and Williams A R 1985 *Phys. Rev. Lett.* **55** 991
[31] Kolesnychenko O Y, Kolesnichenko Y A, Shklyarevskii O I and van Kempen H 2000 *Physica* B **291** 246
[32] Kostov K, Gsell M, Jakob P, Moritz T, Widdra W and Menzel D 1997 *Surf. Sci.* **394** L138–44
[33] Hölzl J, Schulte F K and Wagner H 1979 *Solid Surface Physics* (*Springer Tracts in Modern Physics* vol 85) (Berlin: Springer)
[34] Lide D R 2010 *CRC Handbook of Chemistry and Physics* (Boca Raton, FL: CRC Press)
[35] Włodarczyk R, Sierka M, Sauer J, Löffler D, Uhlrich J J, Yu X, Yang B, Groot I M N, Shaikhutdinov S and Freund H-J 2012 *Phys. Rev.* B **85** 085403
[36] Nilius N, Rienks E D L, Rust H-P and Freund H-J 2005 *Phys. Rev. Lett.* **95** 066101